

Chemical Freeze-out Parameters via a Non-perturbative QCD Approach

Yi Lu,^{1,2,*} Muiyang Chen,³ Zhan Bai,^{1,2,†} Fei Gao,⁴ and Yu-xin Liu^{1,2,5,‡}

¹*Department of Physics and State Key Laboratory of Nuclear Physics and Technology, Peking University, Beijing 100871, China*

²*Collaborative Innovation Center of Quantum Matter, Beijing 100871, China*

³*Department of Physics, Hunan Normal University, Changsha 410081, China*

⁴*Institut für Theoretische Physik, Universität Heidelberg, Philosophenweg 16, 69120 Heidelberg, Germany*

⁵*Center for High Energy Physics, Peking University, Beijing 100871, China*

By analyzing the calculated baryon number susceptibility ratios χ_1^B/χ_2^B and χ_3^B/χ_1^B in two-flavor system via the Dyson-Schwinger equation approach of QCD, we determine the chemical freeze-out temperature and baryon chemical potential in cases of both thermodynamic limit and finite size. We calculate the center-of-mass energy dependence of the χ_4^B/χ_2^B ($\kappa\sigma^2$) at the freeze-out line and find an excellent agreement with experimental data when taking into account the finite size effect. Our calculations indicate that the $\kappa\sigma^2$ exhibits a nonmonotonic behavior in lower collision energy region. We also predict that the collision energy dependence of χ_6^B/χ_2^B is nonmonotonic.

I. INTRODUCTION

Phase transitions of strong interaction matter have been explored for more than forty years since the research may reveal the nature of the early universe matter evolution [1–3]. The transitions include chiral phase transition (from dynamical chiral symmetry to dynamical chiral symmetry breaking) which generates more than 98% of the mass of visible matter and the confinement transition (hadronization) which slaves the quarks and gluons to hadrons. They are driven by the temperature (T) and the baryon density (ρ_B) or chemical potential (μ_B). Since the strong interaction can be well described by Quantum Chromodynamics (QCD), the above mentioned phase transitions are usually referred to as QCD phase transitions. Moreover, many calculations (see, *e.g.*, Refs. [2–19]) have shown that the chiral phase transition at low chemical potential is a crossover at physical quark mass. Theoretical calculations (see, *e.g.*, Refs. [3, 6, 8–19]) also indicate that the chiral phase transition at high chemical potential is first order. Therefore, there would exist a critical end-point (CEP) in the T - μ_B plane at which the first order phase transition turns to crossover. The position of the CEP or even its existence becomes thus one of the most significant topic in both theories and experiments. Besides the efforts in theories, the Beam Energy Scan (BES) program at RHIC, the FAIR at GSI and the NICA at DUBNA all take the search of the CEP as their investigation focus (see, *e.g.*, Refs. [20–22]) and some meaningful information has been provided by the RHIC experiments [23–26].

In experiments, one can measure only the states after the hadronization but not the phase transition directly, and thus the chemical freeze-out line which is defined as the set of states ceasing the inelastic collision of the

newly formed hadrons plays the essential role. Especially, as the chemical freeze-out line approaches to the CEP, nonmonotonic behavior of conserved charge fluctuations could be observed [9, 27–32]. The freeze-out temperature and chemical potential have then been studied in statistical hadronization model (SHM) [33–37], hadron resonance gas (HRG) model [38, 39], lattice QCD simulations [40–43] and other models [44, 45]. In fact, the matter system generated in relativistic heavy ion collision (RHIC) experiment has a finite size and cools in a finite time [30, 31, 46, 47]. The finite size and finite time prevent the correlation length ξ from diverging near the CEP, and smoothen the fluctuations [46]. Model calculations have shown that the finite size influences both the phase diagram and the thermodynamical properties drastically [48–53], the surface of the system may also play the role [54–59]. The effects of the finite size and the surface on the chemical freeze-out parameters will then complement the information for searching the CEP in experiments. However, different models give contradictory results. It is therefore imperative to investigate the finite size and the surface effects on the chemical freeze-out parameters with sophisticated QCD approaches.

It has been known that Dyson-Schwinger equations (DSE), a nonperturbative approach of QCD [60–68], have been successful in describing QCD phase transitions (see, *e.g.*, Refs. [8–13, 64, 69–74]) and hadron properties (For recent reviews, see Refs. [64, 65]). We then, in this paper, take the DSE approach to investigate the chemical freeze-out parameters with the finite size and surface effects being taken into account. We calculate the baryon number susceptibilities in two light-flavor quark system. By comparing the obtained baryon number susceptibility ratios χ_1^B/χ_2^B and χ_3^B/χ_1^B with the experimental data of the net-proton distribution cumulant ratios C_1/C_2 and C_3/C_1 at different collision energies, we determine the freeze-out parameters. We observe that with the finite size and surface effects being included, the calculated collision energy dependence of the χ_4^B/χ_2^B agrees with the experimental data excellently, and the calculated $\kappa\sigma^2$ shows a nonmonotonic behavior in lower collision energy region. Moreover, we propose that hyper-order cumulant

* qwertylou@pku.edu.cn

† Present address: Institute of Theoretical Physics, Chinese Academy of Science, Beijing 100081, China

‡ Corresponding author: yxliu@pku.edu.cn

ratio such as χ_6^B/χ_2^B also shows a nonmonotonic dependence on the collision energy.

The remainder of this paper is organized as follows: In Sec. II, we describe briefly the Dyson-Schwinger equation approach and its relation to the chemical freeze-out parameters. In Sec. III, we calculate the freeze-out parameters by adopting the DSE approach as well as the experimental data. In Sec. IV, we give the phase diagram in the vicinity of CEP and reveal the effect of finite size and surface. In Sec. V, we give a summary and discussion.

II. THEORETICAL FRAMEWORK.

A. Dyson-Schwinger Equation Approach

The Dyson-Schwinger equations are infinite number of coupled equations. In this paper, we focus on the DSE for quark propagator $S(\tilde{\omega}_j, \vec{p})$. The corresponding equation is:

$$S^{-1}(\tilde{\omega}_j, \vec{p}) = Z_2 (i\vec{\gamma} \cdot \vec{p} + i\gamma_4 \tilde{\omega}_j) + Z_4 m_0 + Z_1 \Sigma(\tilde{\omega}_j, \vec{p}), \quad (1)$$

where Z_1 , Z_2 and Z_4 are renormalization constants. m_0 is the current quark mass. $\tilde{\omega}_j = \omega_j + i\mu_q$, with μ_q being the quark chemical potential, and $\omega_j = (2j+1)\pi T$ the Matsubara frequency for quarks. $\Sigma(\tilde{\omega}_j, \vec{p})$ is the self-energy of quark, and reads:

$$\begin{aligned} \Sigma(\tilde{\omega}_j, \vec{p}) = & \frac{4}{3} T \sum_{l=-\infty}^{\infty} \int \frac{d^3 \vec{q}}{(2\pi)^3} g^2 D_{\mu\nu}(\vec{k}, \Omega_{jl}; T, \mu_q) \\ & \times \gamma_\mu S(\tilde{\omega}_l, \vec{q}) \Gamma_\nu(\vec{p}, \tilde{\omega}_j, \vec{q}, \tilde{\omega}_l; T, \mu_q), \end{aligned} \quad (2)$$

where $D_{\mu\nu}$ is the dressed-gluon propagator, Γ_ν is the dressed quark-gluon vertex, $\Omega_{jl} = \omega_j - \omega_l$ is the Matsubara frequency for gluon.

In principle, the gluon propagator $D_{\mu\nu}$ and the quark-gluon vertex Γ_ν should be solved by corresponding DSEs, which depend on higher order correlation functions. And a truncation must be applied in order for numerical solution. In this paper, for the quark-gluon vertex, we adopt at first stage the rainbow approximation for the vertex $\Gamma_\nu(\vec{p}, \tilde{\omega}_m, \vec{q}, \tilde{\omega}_l; T, \mu_q) = \gamma_\nu$.

The gluon propagator has the general form

$$g^2 D_{\mu\nu}(\Omega_{nl}, \vec{k}) = P_{\mu\nu}^T D_T(\Omega_{nl}^2, \vec{k}^2) + P_{\mu\nu}^L D_L(\Omega_{nl}^2, \vec{k}^2), \quad (3)$$

where $P_{\mu\nu}^{T,L}$ are the transverse and longitudinal projection operators, respectively:

$$\begin{aligned} P_{\mu\nu}^T &= (1 - \delta_{\mu 4})(1 - \delta_{\nu 4}) \left(\delta_{\mu\nu} - \frac{k_\mu k_\nu}{k^2} \right), \\ P_{\mu\nu}^L &= \left(\delta_{\mu\nu} - \frac{k_\mu k_\nu}{k^2} \right) - P_{\mu\nu}^T, \end{aligned} \quad (4)$$

where $k = (\Omega_{nl}, \vec{k})$. D_T and D_L are the effective interactions and can be represented using models. Note that

the coupling constant g and the renormalization constant Z_1 has been absorbed into the effective interaction.

In this paper, we adopt the infrared constant model (QC model) [9, 13, 68], which reads:

$$\mathcal{D}(s) = 8\pi^2 \frac{D}{\omega^4} e^{-s/\omega^2} + \alpha_{\text{pQCD}}(s), \quad (5)$$

where D and ω are the parameters of the model. α_{pQCD} is the ultraviolet perturbation term and reads:

$$\alpha_{\text{pQCD}}(s) = \frac{8\pi^2 \gamma_m}{\ln \left[\tau + \left(1 + s/\Lambda_{\text{QCD}}^2 \right)^2 \right]} \mathcal{F}(s), \quad (6)$$

where $\mathcal{F}(s) = [1 - \exp(-s/4m_t^2)]$, $\tau = e^2 - 1$, $m_t = 0.5$ GeV, $\Lambda_{\text{QCD}} = 0.234$ GeV, and $\gamma_m = 12/(33 - N_f)$ with $N_f = 4$.

The gluon screening mass m_g is also considered in the longitudinal part of gluon model [13, 75]:

$$\begin{aligned} D_T(\Omega_{nl}^2, \vec{k}^2) &= \mathcal{D}(\Omega_{nl}^2 + \vec{k}^2), \\ D_L(\Omega_{nl}^2, \vec{k}^2) &= \mathcal{D}(\Omega_{nl}^2 + \vec{k}^2 + m_g^2), \end{aligned} \quad (7)$$

whose value is determined by leading-order perturbative QCD [76]:

$$m_g^2 = \frac{16}{5} \left(T^2 + \frac{6}{5\pi^2} \mu_q^2 \right). \quad (8)$$

In order to fix the renormalization constant Z_2 and Z_4 , we need to specify the renormalization condition. In this paper, the renormalization condition is:

$$S^{-1}(p^2) \Big|_{\omega_0^2 + \vec{p}^2 = \zeta^2} = i(\vec{\gamma} \cdot \vec{p} + \gamma_4 \tilde{\omega}_0) + m_0, \quad (9)$$

where ζ is the renormalization point. We choose $\zeta = 19$ GeV, $m_0 = 3.4$ MeV, $D = 1.024$ GeV² and $\omega = 0.5$ GeV as in Ref. [68].

The quark propagator can be decomposed according to its Lorentz structure. At finite temperature, the decomposition is:

$$\begin{aligned} S(\tilde{\omega}_j, \vec{p})^{-1} &= i\vec{\gamma} \cdot \vec{p} A(\tilde{\omega}_j^2, \vec{p}^2) \\ &+ i\gamma_4 \tilde{\omega}_j C(\tilde{\omega}_j^2, \vec{p}^2) + B(\tilde{\omega}_j^2, \vec{p}^2). \end{aligned} \quad (10)$$

There should be, in principle, a fourth term in this decomposition. However, its contribution to order parameter is extremely small and is usually omitted in practical calculations [61, 77].

The mass function of the quark propagator can then be defined as:

$$M(\tilde{\omega}_j^2, \vec{p}^2) = B(\tilde{\omega}_j^2, \vec{p}^2)/A(\tilde{\omega}_j^2, \vec{p}^2). \quad (11)$$

In vacuum, the physical solution to the quark DSE has a non-zero mass function even if the current quark mass is zero. At high temperature, the mass function gradually approaches the current quark mass. Therefore, the mass function at zero momentum, $M(\tilde{\omega}_0^2, 0)$, is often used as the order parameter of the QCD crossover.

B. Number Density and susceptibilities

Experimental observations indicate that the yields of pion and proton are much larger than that of kaon [36], we can then simplify the matter generated in RHIC experiments as that including mainly two light flavor quarks. In the system of u and d quarks, baryon number density n_B and electric charge density n_Q can be fixed with quark number density $n_{u,d}$ as:

$$n_B = \frac{1}{3}n_u + \frac{1}{3}n_d, \quad n_Q = \frac{2}{3}n_u - \frac{1}{3}n_d. \quad (12)$$

From Eq. (12) we notice that the u and d quarks are in exact isospin symmetry, if only the baryon number is considered. In this sense, both the u quark and d quark hold the same quark chemical potential $\mu_q = \mu_B/3$, and the quark number density $n_q = 3n_B$.

In view of statistical physics, the quark number density can be determined as

$$n_q(\mu_q, T) = 2N_c N_f Z_2 \int \frac{d^3\vec{p}}{(2\pi)^3} f_1(|\vec{p}|; \mu_q, T), \quad (13)$$

$$f_1(|\vec{p}|; \mu_q, T) = \frac{T}{2} \sum_{j=-\infty}^{\infty} \text{tr}_D [-\gamma_4 S(\tilde{\omega}_j, \vec{p})], \quad (14)$$

where Z_2 is the quark wave-function renormalization constant, $N_c = 3$ the color number, and $N_f = 2$ the flavor number. Notice that the flavor number here represents the flavor degeneracy, and is different from the one we used in the ultraviolet perturbation term in the gluon model.

In Eq. (14), the summation runs over an infinite number of Matsubara frequencies. In practice, we can only carry out the calculation with a finite number of Matsubara frequency, and the summation must have a cut-off, N . However, the convergence of summation Eq. (14) is slow, especially at low temperature. On the other hand, we observe that the scalar functions A , B and C defined in Eq. (10) converge quickly to the free-quark-propagator scalar functions $A = C = 1$, $B = m_0$, as the Matsubara frequency grows large. For free propagator, the distribution function is:

$$\begin{aligned} f^{\text{free}}(|\vec{p}|; \mu_q, T) &= \frac{T}{2} \sum_{j=-\infty}^{\infty} \text{tr}_D [-\gamma_4 S^{\text{free}}(\tilde{\omega}_j, \vec{p})] \\ &= \frac{1}{e^{(E-\mu_q)/T} + 1} - \frac{1}{e^{(E+\mu_q)/T} + 1}, \end{aligned} \quad (15)$$

where $E = \sqrt{\vec{p}^2 + m_0^2}$.

Therefore, the contribution of missing Matsubara frequencies that exceed the cut-off N in Eq. (14), can be approximated using the distribution function of free prop-

agator:

$$\begin{aligned} f_1 &= \frac{T}{2} \sum_{j=-N}^N \text{tr}_D [-\gamma_4 S(\tilde{\omega}_j, \vec{p})] \\ &+ f^{\text{free}} - \frac{T}{2} \sum_{j=-N}^N \text{tr}_D [-\gamma_4 S^{\text{free}}(\tilde{\omega}_j, \vec{p})]. \end{aligned} \quad (16)$$

Using this technique, the calculated quark number density has better convergence at moderate and high temperature, whose chemical potential dependence is shown in Fig. 1.

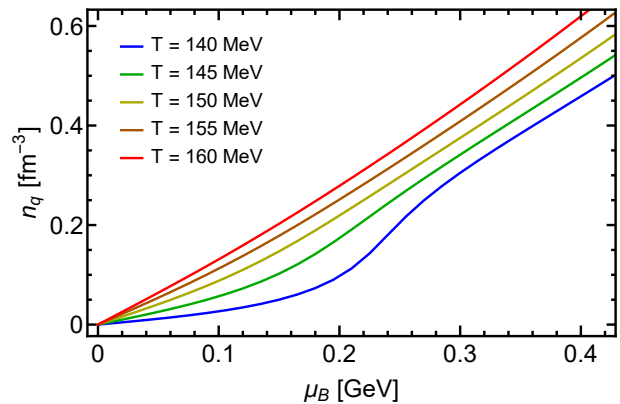


FIG. 1. Calculated baryon chemical potential dependence of the quark number density at some values of given temperature, in case of thermodynamical limit using Eq. (16).

After calculating the quark number density, we can calculate the susceptibility by taking derivatives. The k th order baryon number density susceptibility (fluctuation) is obtained as

$$\begin{aligned} \chi_1^B &= n_B, \\ \chi_k^B &= \frac{1}{\beta^{(k-1)}} \frac{\partial^{(k-1)} n_B}{\partial^{(k-1)} \mu_B}, \end{aligned} \quad (17)$$

where $\beta = 1/T$ and $k = 2, 3, 4, \dots$. The susceptibilities are related to the moments of the multiplicity distributions of the corresponding conserved charges as

$$\begin{aligned} \frac{\chi_1}{\chi_2} &= M/\sigma^2, & \frac{\chi_3}{\chi_1} &= S\sigma^3/M, \\ \frac{\chi_3}{\chi_2} &= S\sigma, & \frac{\chi_4}{\chi_2} &= \kappa\sigma^2, \end{aligned} \quad (18)$$

where M , σ^2 , S and κ are the mean, the variance, the skewness and the kurtosis of the multiplicity distribution, respectively. By comparing the theoretical net-baryon number fluctuations in terms of temperature and chemical potential with the experimental data one can determine the freeze-out parameters [43].

C. Finite Size and Surface Effect

The system created in RHIC exists in finite size, rather than thermodynamical limit. To determine the freeze-out parameters in experiment one has to take the finite size and the surface effects into account. Assuming the system as a cube of size L , and adopting the anti-periodic condition, the momentum of a fermion should be $p_j = (2j + 1)\pi/L$. In principle, one should sum over discrete momentum values. For simplicity, the finite size effect is roughly incorporated by a non-zero momentum cut-off $|p|_{\min} = \pi/L$ [51, 52]. It corresponds to an infrared momentum cut-off in Eqs. (1) and (13). This can also be understood by the quantum uncertainty principle, that L^{-1} is the energy scale for a system of finite size L . It is remarkable that such an L is not exactly the same as the size of fireball, but an effective scale that the ingredients of the quark matter can interact.

We also incorporate the effect of the surface through the multiple reflection expansion (MRE) approximation. In the MRE approximation, the thermodynamical quantities of a droplet composed of quarks can be derived from a density of states in the form [54–56, 78, 79]

$$\frac{dN}{dp} = 6 \left[\frac{p^2 V}{2\pi^2} + f_s \left(\frac{p}{M} \right) pS + f_c \left(\frac{p}{M} \right) C + \dots \right], \quad (19)$$

where V is the volume of the droplet, $S = 4\pi L^2$ and $C = 8\pi L$ are the area, the extrinsic curvature of the surface of the droplet, respectively. The f_s and f_c are the contributions to the density of states from the surface and curvature, given explicitly as [50, 78]:

$$f_s \left(\frac{p}{M} \right) = -\frac{1}{8\pi} \left(1 - \frac{2}{\pi} \arctan \left(\frac{p}{M} \right) \right), \quad (20)$$

$$f_c \left(\frac{p}{M} \right) = \frac{1}{12\pi^2} \left[1 - \frac{3p}{2M} \left(\frac{\pi}{2} - \arctan \left(\frac{p}{M} \right) \right) \right],$$

with p being the momentum and M the constituent quark mass.

Rigorously, one should solve the coupled equations for the constituent mass M [50]. For simplicity we set M in Eq. (19) to be $M = \text{Re } M(\tilde{\omega}_0^2, 0)$ from the mass function defined in Eq. (11), calculated from Eq. (1) with a finite system size L .

The modified density of states is then [50, 79]:

$$\rho_{\text{MRE}}(p, M, L) = 1 + \frac{6\pi^2}{pL} f_s + \frac{12\pi^2}{(pL)^2} f_c. \quad (21)$$

After taking into account the finite-size as well as the surface effect, the momentum integration in Sec. II A should be converted as follows:

$$\int_0^\infty \frac{\vec{p}^2 dp}{2\pi^2} \longrightarrow \int_{|p|_{\min}}^\Lambda \rho_{\text{MRE}} \frac{\vec{p}^2 dp}{2\pi^2}. \quad (22)$$

III. FREEZE-OUT PARAMETERS

We have carried out calculations with $L = \infty$ (thermodynamical limit) and various finite values of L . The calculations manifest that the fluctuations (skewness, kurtosis, etc.) in the T - μ_B plane behave qualitatively the same as those given in Ref. [9], respectively. The obtained μ_B dependence of the baryon number susceptibility ratios χ_1^B/χ_2^B and χ_3^B/χ_1^B in case of $L = 2.2$ fm at several values of temperature are shown in Fig. 2. It is evident that our results agree with the lattice QCD results [43] qualitatively very well. In order to extract the freeze-out parameters, we plot the experimental values of the cumulant ratios $C_1/C_2 = M/\sigma^2$ and $C_3/C_1 = S\sigma^3/M$ of net-proton multiplicity distributions in central collisions [26] as horizontal lines.

By fitting our calculated χ_1^B/χ_2^B and χ_3^B/χ_1^B values in terms of T and μ_B with the experimental data we get the freeze-out parameters (μ_B^f, T^f) . The obtained results when $L = \infty, 3.5$ fm, 2.8 fm, 2.5 fm and 2.2 fm are

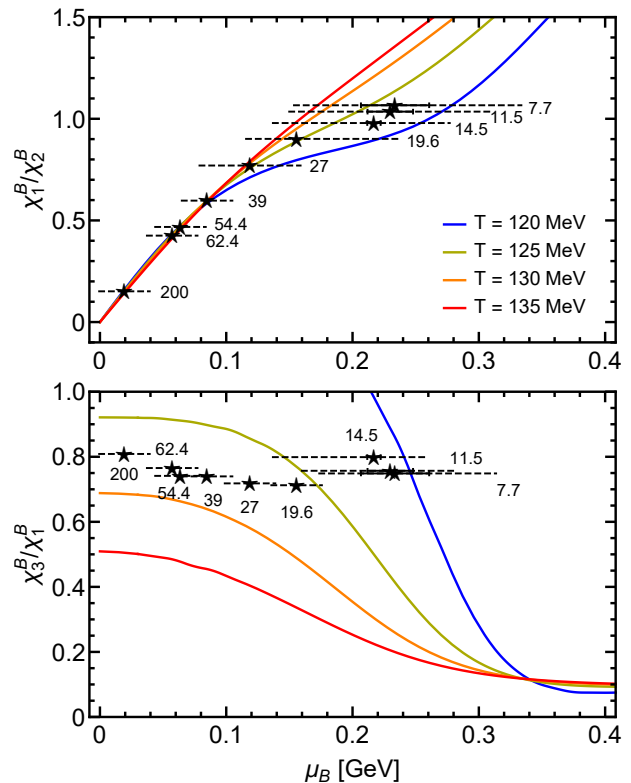


FIG. 2. (color online) Calculated baryon chemical potential dependence of the fluctuation ratios χ_1^B/χ_2^B (upper panel) and χ_3^B/χ_1^B (lower panel) of the system with $L = 2.2$ fm at several values of temperature near the T_c . The dashed horizontal lines stand for the experimental values of the efficiency-corrected $C_1/C_2 = M/\sigma^2$ and $C_3/C_1 = S\sigma^3/M$ of net-proton multiplicity distributions in the central collisions at $\sqrt{S_{NN}} = 200, 62.4, 54.4, 39, 27, 19.6, 14.5, 11.5, 7.7$ GeV given in Ref. [26]. The stars label our assigned freeze-out points.

TABLE I. Calculated freeze-out points (μ_B^f, T^f) in case of different values of L (T^f and μ_B^f are in unit MeV and $\sqrt{S_{NN}}$ in GeV).

$\sqrt{S_{NN}}$	$L = \text{infinity}$		$L = 3.5 \text{ fm}$		$L = 2.8 \text{ fm}$		$L = 2.5 \text{ fm}$		$L = 2.2 \text{ fm}$	
	μ_B^f	T^f	μ_B^f	T^f	μ_B^f	T^f	μ_B^f	T^f	μ_B^f	T^f
200	23.7	155.5	22.8	150.0	21.9	144.1	21.1	138.8	19.4	127.5
62.4	69.9	155.1	67.1	150.0	64.4	144.0	62.1	138.9	57.2	128.0
54.4	77.2	155.1	74.6	150.0	70.2	144.3	69.1	139.1	63.8	128.4
39	103.3	154.2	99.5	149.2	95.5	143.5	92.0	138.5	84.8	128.1
27	154.7	150.7	143.0	147.1	135.4	141.8	129.6	137.3	118.8	127.5
19.6	189.1	148.0	191.7	143.1	195.2	137.5	178.7	134.1	155.7	126.0
	± 15.7	± 1.9	± 10.9	± 1.2	± 2.5	± 0.2				
14.5	—	—	—	—	241.5	132.0	203.3	131.6	217.0	121.9
					± 21.1	± 2.7	± 23.8	± 2.2	± 5.3	± 0.4
11.5	—	—	—	—	—	—	255.0	127.7	229.9	121.4
							± 34.3	± 2.3	± 18.0	± 1.4
7.7	—	—	—	—	—	—	257.4	127.5	233.7	121.2
							± 39.9	± 2.9	± 27.0	± 2.1

listed in Table I. It appears that our theoretical results in the thermodynamical limit ($L = \infty$) do not fit the experimental values well at low collision energy, whereas the deviations are smaller if the finite size parameter L changes.

We illustrate the presently calculated relation between the baryon chemical potential μ_B^f and the center-of-mass energy of the collision, $\sqrt{S_{NN}}$, and the comparison with those given in lattice QCD simulations (*e.g.*, Ref. [43]) and model calculations (*e.g.*, Refs. [34, 39]) in Fig. 3. We see from Fig. 3 that our freeze-out baryon chemical potential in case of $L = \infty$ and that when $L = 2.2 \text{ fm}$ match the lattice QCD result and model calculation results well in the region $\mu_B < 100 \text{ MeV}$, while those in case of $L = 2.2 \text{ fm}$ deviate from previous results in the

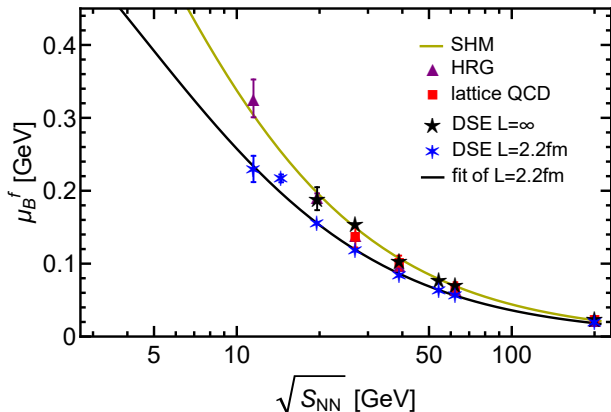


FIG. 3. (color online) Comparison of presently obtained $\sqrt{S_{NN}}$ dependence of the baryon chemical potential in cases of $L = \infty$ and $L = 2.2 \text{ fm}$ with those given in lattice QCD simulation [43], HRG model [39] and the parameterized one in SHM model [34].

TABLE II. Fitted freeze-out parameters c, d in Eq. 23 and T^0, a, b in Eq. 24, in case of different finite size parameter L (c and T^0 are in unit MeV and d in GeV^{-1}).

L	c	d	T^0	a	b
infinity	1642.8	0.373	155.7	0.0162	0.0166
3.5 fm	1236.1	0.285	150.3	0.0130	0.0103
2.8 fm	1066.9	0.256	144.6	0.0184	0.0043
2.5 fm	840.9	0.205	139.2	0.0137	0.0051
2.2 fm	818.4	0.218	128.4	0.0106	0.0022

$\mu_B > 100 \text{ MeV}$ range. With the obtained freeze-out points, the freeze-out conditions are fitted as:

$$\mu_B^f = \frac{c}{1 + d\sqrt{S_{NN}}}, \quad (23)$$

$$T^f = T^0 \left[1 - a \left(\frac{\mu_B^f}{T^0} \right)^2 - b \left(\frac{\mu_B^f}{T^0} \right)^4 \right]. \quad (24)$$

Only the freeze-out points with small deviation between theory and experiment in Table I are used for fitting the freeze-out conditions, and the obtained best-fitted parameters are listed in Table II. The fitted $\mu_B^f(\sqrt{S_{NN}})$ curve is also displayed in Fig. 3.

With the parametrization, one can predict the freeze-out parameters (μ_B^f, T^f) of the system generated in any collision energy. For example, with $L = 2.2 \text{ fm}$, $\sqrt{S_{NN}} = 5.8 \text{ GeV}$, 7.7 GeV , 11.5 GeV , 14.5 GeV correspond to $(\mu_B^f, T^f) = (361.7, 99.6) \text{ MeV}$, $(305.8, 111.5) \text{ MeV}$, $(233.6, 120.8) \text{ MeV}$, $(196.9, 123.6) \text{ MeV}$, respectively.

IV. PHASE DIAGRAM AND FURTHER PREDICTION

With the quark propagator obtained by solving the DSE, we can get the temperature and chemical potential dependence of the quark condensate and the quark dynamical mass, which are commonly regarded as appropriate order parameters of chiral phase transition. Taking the chiral susceptibility criterion [8, 75] we determine the upper and lower boundary of the chiral phase crossover region by the full width at half maxima (FWHM) of the susceptibility. The chiral susceptibility is defined as:

$$\chi_T = -\partial M(\tilde{\omega}_0^2, 0)/\partial T, \quad (25)$$

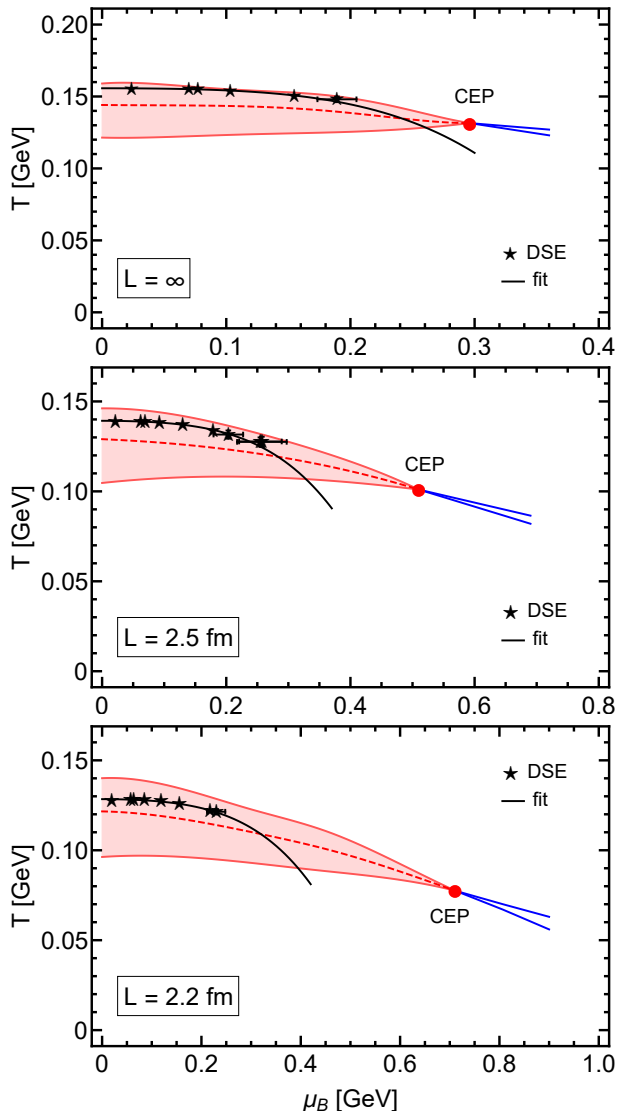


FIG. 4. (color online) Calculated QCD phase diagram in case of $L = \infty$, 2.5 fm and 2.2 fm. The red-dashed curves are the phase boundaries defined with the maximum of chiral susceptibility, the red-colored areas are the obtained crossover regions, and the black-solid curves are the fitted freeze-out lines.

where the constituent quark mass is defined as the real part of $M(\tilde{\omega}_0^2, 0)$ in Eq. (11), the same as in Sec. II C.

The obtained crossover regions in cases of $L = \infty$, 2.5 fm and 2.2 fm are shown as the shadowed regions in Fig. 4. With the chiral susceptibility criterion [8, 75] or the fluctuation criterion [9], we determine the boundaries of the first order transition region and the location of the CEP. The obtained results in the two cases are displayed in Fig. 4. We illustrate also the presently obtained chemical freeze-out lines in these cases in Fig. 4. The figure manifests that the chemical freeze-out happens in the obtained chiral crossover region. Quantitatively, the freeze-out temperature $T^f = 155.7$ MeV is higher than the $T_c = 144.0$ MeV in the thermodynamical limit (*i.e.*, with $L = \infty$) at $\mu_B = 0$, but the deviation is smaller in case of $L = 2.2$ fm where $T^f = 128.4$ MeV, $T_c = 121.6$ MeV at $\mu_B = 0$. We also notice that the finite size effect shifts the location of the CEP to higher baryon chemical potential and lower temperature drastically: in case of $L = \infty$, 3.5 fm, 2.8 fm, 2.5 fm and 2.2 fm, $(\mu_B^{\text{CEP}}, T^{\text{CEP}}) = (296, 132)$, $(360, 121)$, $(426, 111)$, $(510, 101)$, $(711, 77.5)$ MeV, respectively. This is consistent with the behavior given in phenomenological model calculations [48, 51]. Compared with the location of CEP calculated from functional renormalization group (FRG) approach [80, 81], it indicates that the inclusion of the finite size effect is reasonable for $2.2 \text{ fm} \leq L \leq 2.8 \text{ fm}$.

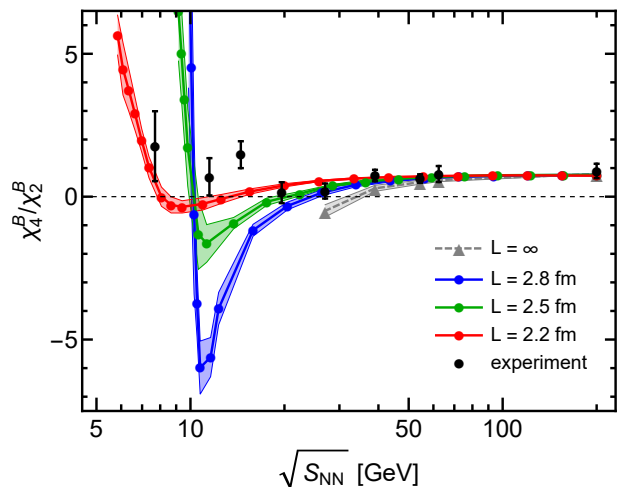


FIG. 5. (color online) Calculated collision energy $\sqrt{S_{NN}}$ dependence of $\kappa\sigma^2 = \chi_4^B/\chi_2^B$ at the freeze-out line. The black circles are the experimental values [26], the gray triangles stand for our results in case of infinite volume, the blue, green and red points denote our results in the case of $L = 2.8$ fm, 2.5 fm and 2.2 fm respectively. The shadowed region(s) displays the numerical uncertainties.

It is known that the $\kappa\sigma^2 = \chi_4/\chi_2$ is a direct observable in experiment and may demonstrate the property of the states around the CEP well. We calculate χ_4^B/χ_2^B in the $T-\mu_B$ plane and pick out the value along the freeze-out line to get the $\sqrt{S_{NN}}$ dependence of χ_4^B/χ_2^B . The obtained results in case of thermodynamical limit, finite

size of $L = 2.8$ fm, 2.5 fm and 2.2 fm are depicted in Fig. 5. In case of $L = 2.2$ fm, the lowest collision energy calculated is 5.8 GeV. It is apparent that, without considering the finite size effect, our calculated χ_4^B/χ_2^B decreases more rapidly than the experimental data as the $\sqrt{S_{NN}}$ descends. With the finite size effect being taken into account, we can reproduce the experimental data excellently. In the lower collision energy region, the $\kappa\sigma^2$ exhibits a nonmonotonic behavior, whose minimum is reached at $\sqrt{S_{NN}} \approx 10$ GeV, and then increases drastically as $\sqrt{S_{NN}}$ further decreases.

Since the calculated kurtosis fit the experimental data best in case of $L = 2.2$ fm, we further calculate the $\sqrt{S_{NN}}$ dependence of χ_6^B/χ_2^B from our fitted freeze-out line under this finite size parameter, depicted in Fig. 6, whose numerical uncertainties are much larger than the results of $\kappa\sigma^2$ though.

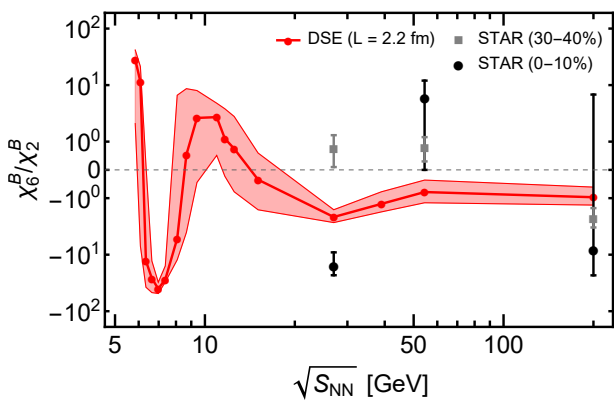


FIG. 6. (color online) Calculated collision energy $\sqrt{S_{NN}}$ dependence of χ_6^B/χ_2^B (in logarithmic scale) at the freeze-out line. The black circles and gray squares are the experimental values [82] for 0-10% and 30-40% centralities respectively, and the red points denote our results in case of 2.2 fm. The shadowed region(s) displays the numerical uncertainties.

At $\sqrt{S_{NN}} = 200$ GeV, we obtain a negative value of

$\chi_6^B/\chi_2^B = -0.97 \pm 0.36$, which is qualitatively consistent with the experimental results [82–84] and lattice calculation [85]. For $\sqrt{S_{NN}} \gtrsim 10$ GeV, our result shows a non-monotonic behavior with a shallow minimum, in agreement with the FRG calculation [86]. We also show that χ_6^B/χ_2^B may have a large maximum along with a sharp and deep minimum when $\sqrt{S_{NN}} \lesssim 10$ GeV. As a result, we predict a complex nonmonotonic behavior of χ_6^B/χ_2^B as a function of collision energy.

V. SUMMARY

In summary, we have calculated in this work the baryon number susceptibilities in a two-flavor quark system via the DSE approach of QCD in case of not only thermodynamic limit but also finite size. By comparing the calculated ratios χ_1^B/χ_2^B and χ_3^B/χ_1^B with the experimental data of the net-proton multiplicity distribution in BES at RHIC, we obtained the temperature and the baryon chemical potential at the chemical freeze-out states. We calculated also the collision energy dependence of the $\kappa\sigma^2$ at the freeze-out line and observed an excellent agreement with experimental data when taking into account the finite size effect. It shows that the finite size effect is significant in studying the QCD phase transitions with RHICs. The obtained collision energy $\sqrt{S_{NN}}$ dependence of the $\kappa\sigma^2$ exhibits a nonmonotonic behavior in lower collision energy region. We also predict that the collision energy dependence of hyper-order cumulant ratios such as χ_6^B/χ_2^B may also be nonmonotonic.

ACKNOWLEDGMENTS

The work was supported by the National Natural Science Foundation of China under Grant Nos. 11175004 and 11435001, and the National Key Basic Research Program of China under Grant No. 2015CB856900.

-
- [1] P. Braun-Munzinger and J. Wambach, *Rev. Mod. Phys.* **81**, 1031 (2009), arXiv:0801.4256.
 - [2] O. Philipsen, *Prog. Part. Nucl. Phys.* **70**, 55 (2013), arXiv:1207.5999.
 - [3] S. Gupta, X. Luo, B. Mohanty, H. G. Ritter, and N. Xu, *Science* **332**, 1525 (2011), arXiv:1105.3934.
 - [4] Y. Aoki, G. Endrődi, Z. Fodor, S. D. Katz, and K. K. Szabó, *Nature* **443**, 675 (2006), arXiv:hep-lat/0611014.
 - [5] Y. Aoki, S. Borsányi, S. Dürr, Z. Fodor, S. D. Katz, S. Krieg, and K. Szabo, *J. High Energy Phys.* **2009**, 088 (2009), arXiv:0903.4155.
 - [6] S. Ejiri, *Phys. Rev. D* **78**, 074507 (2008), arXiv:0804.3227.
 - [7] A. Li, A. Alexandru, and K.-F. Liu, *Phys. Rev. D* **84**, 071503 (2011), arXiv:1103.3045.
 - [8] S. X. Qin, L. Chang, H. Chen, Y. X. Liu, and C. D. Roberts, *Phys. Rev. Lett.* **106**, 172301 (2011), arXiv:1011.2876.
 - [9] X. Y. Xin, S. X. Qin, and Y. X. Liu, *Phys. Rev. D* **90**, 076006 (2014).
 - [10] C. S. Fischer, J. Luecker, and J. A. Mueller, *Phys. Lett. B* **702**, 438 (2011), arXiv:1104.1564.
 - [11] C. S. Fischer and J. Luecker, *Phys. Lett. B* **718**, 1036 (2013), arXiv:1206.5191.
 - [12] C. S. Fischer, J. Luecker, and C. A. Welzbacher, *Phys. Rev. D* **90**, 034022 (2014), arXiv:1405.4762.
 - [13] F. Gao, J. Chen, Y. X. Liu, S. X. Qin, C. D. Roberts, and S. M. Schmidt, *Phys. Rev. D* **93**, 094019 (2016), arXiv:1507.00875.

- [14] C. Ratti, M. A. Thaler, and W. Weise, *Phys. Rev. D* **73**, 014019 (2006), arXiv:hep-ph/0506234.
- [15] B.-J. Schaefer, J. M. Pawłowski, and J. Wambach, *Phys. Rev. D* **76**, 074023 (2007), arXiv:0704.3234.
- [16] W. J. Fu, Z. Zhang, and Y. X. Liu, *Phys. Rev. D* **77**, 014006 (2008), arXiv:0711.0154.
- [17] K. Fukushima, *Phys. Rev. D* **77**, 114028 (2008), arXiv:0803.3318.
- [18] L. J. Jiang, X. Y. Xin, K. L. Wang, S. X. Qin, and Y. X. Liu, *Phys. Rev. D* **88**, 016008 (2013).
- [19] X. Y. Xin, S. X. Qin, and Y. X. Liu, *Phys. Rev. D* **89**, 094012 (2014).
- [20] G. L. Melkumov *et al.* (NA49), *Nucl. Phys. B Proc. Suppl.* **219-220**, 102 (2011).
- [21] G. L. Melkumov *et al.* (NA49), *Phys. Atom. Nucl.* **75**, 556 (2012).
- [22] G. Odyniec, *Phys. Atom. Nuclei* **75**, 602 (2012).
- [23] L. Adamczyk *et al.* (STAR), *Phys. Rev. Lett.* **112**, 032302 (2014), arXiv:1309.5681.
- [24] L. Adamczyk *et al.* (STAR), *Phys. Rev. Lett.* **113**, 092301 (2014), arXiv:1402.1558 [nucl-ex].
- [25] X. Luo, *PoS CPOD2014*, 019 (2015), arXiv:1503.02558.
- [26] J. Adam *et al.* (STAR), *Phys. Rev. Lett.* **126**, 092301 (2021).
- [27] M. Stephanov, K. Rajagopal, and E. Shuryak, *Phys. Rev. Lett.* **81**, 4816 (1998), arXiv:hep-ph/9806219.
- [28] M. A. Stephanov, *Phys. Rev. Lett.* **102**, 032301 (2009), arXiv:0809.3450.
- [29] M. A. Stephanov, *Phys. Rev. Lett.* **107**, 052301 (2011), arXiv:1104.1627.
- [30] M. Stephanov, K. Rajagopal, and E. Shuryak, *Phys. Rev. D* **60**, 114028 (1999), arXiv:hep-ph/9903292.
- [31] M. A. Stephanov, *J. Phys. G* **38**, 124147 (2011).
- [32] Y. Hatta and M. A. Stephanov, *Phys. Rev. Lett.* **91**, 102003 (2003), arXiv:hep-ph/0302002.
- [33] F. Becattini, J. Manninen, and M. Gaździcki, *Phys. Rev. C* **73**, 044905 (2006), arXiv:hep-ph/0511092.
- [34] A. Andronic, P. Braun-Munzinger, and J. Stachel, *Nucl. Phys. A* **772**, 167 (2006), arXiv:nucl-th/0511071.
- [35] A. Andronic, P. Braun-Munzinger, and J. Stachel, *Physics Letters B* **673**, 142 (2009), arXiv:0812.1186.
- [36] S. Das and (the STAR collaboration), *J. Phys.: Conf. Ser.* **509**, 012066 (2014), arXiv:1402.0255.
- [37] S. Das, *EPJ Web Conf.* **90**, 10003 (2015), arXiv:1412.0350.
- [38] F. Karsch and K. Redlich, *Phys. Lett. B* **695**, 136 (2011), arXiv:1007.2581.
- [39] P. Alba, W. Alberico, R. Bellwied, M. Bluhm, V. Mantovani Sarti, M. Nahrgang, and C. Ratti, *Phys. Lett. B* **738**, 305 (2014), arXiv:1403.4903.
- [40] R. V. Gavai and S. Gupta, *Phys. Lett. B* **696**, 459 (2011), arXiv:1001.3796.
- [41] A. Bazavov, H.-T. Ding, P. Hegde, O. Kaczmarek, F. Karsch, E. Laermann, S. Mukherjee, P. Petreczky, C. Schmidt, D. Smith, W. Soeldner, and M. Wagner, *Phys. Rev. Lett.* **109**, 192302 (2012), arXiv:1208.1220.
- [42] S. Borsányi, Z. Fodor, S. D. Katz, S. Krieg, C. Ratti, and K. K. Szabó, *Phys. Rev. Lett.* **111**, 062005 (2013), arXiv:1305.5161.
- [43] S. Borsányi, Z. Fodor, S. D. Katz, S. Krieg, C. Ratti, and K. K. Szabo, *Phys. Rev. Lett.* **113**, 052301 (2014), arXiv:1403.4576.
- [44] J. Cleymans, H. Oeschler, K. Redlich, and S. Wheaton, *Phys. Rev. C* **73**, 034905 (2006), arXiv:hep-ph/0511094.
- [45] J.-W. Chen, J. Deng, H. Kohyama, and L. Labun, *Phys. Rev. D* **93**, 034037 (2016), arXiv:1509.04968.
- [46] B. Berdnikov and K. Rajagopal, *Phys. Rev. D* **61**, 105017 (2000), arXiv:hep-ph/9912274.
- [47] B. B. Abelev *et al.* (ALICE), *Phys. Lett. B* **739**, 139 (2014), arXiv:1404.1194 [nucl-ex].
- [48] L. F. Palhares, E. S. Fraga, and T. Kodama, *J. Phys. G* **38**, 085101 (2011), arXiv:0904.4830 [nucl-th].
- [49] N. Magdy, M. Csanád, and R. A. Lacey, *J. Phys. G* **44**, 025101 (2017), arXiv:1510.04380 [nucl-th].
- [50] G. Y. Shao, L. Chang, Y. X. Liu, and X. L. Wang, *Phys. Rev. D* **73**, 076003 (2006), arXiv:hep-ph/0602100.
- [51] A. Bhattacharyya, P. Deb, S. K. Ghosh, R. Ray, and S. Sur, *Phys. Rev. D* **87**, 054009 (2013), arXiv:1212.5893 [hep-ph].
- [52] A. Bhattacharyya, R. Ray, and S. Sur, *Phys. Rev. D* **91**, 051501 (2015), arXiv:1412.8316 [hep-ph].
- [53] A. Bhattacharyya, S. K. Ghosh, R. Ray, K. Saha, and S. Upadhaya, *EPL* **116**, 52001 (2016), arXiv:1507.08795 [hep-ph].
- [54] M. S. Berger and R. L. Jaffe, *Phys. Rev. C* **35**, 213 (1987).
- [55] D. Deutsch and P. Candelas, *Phys. Rev. D* **20**, 3063 (1979).
- [56] H. T. Elze and W. Greiner, *Phys. Lett. B* **179**, 385 (1986).
- [57] W. Y. Ke and Y. X. Liu, *Phys. Rev. D* **89**, 074041 (2014), arXiv:1312.2295 [hep-ph].
- [58] F. Gao and Y. X. Liu, *Phys. Rev. D* **94**, 094030 (2016), arXiv:1609.08038 [hep-ph].
- [59] Y. P. Zhao, R. R. Zhang, H. Zhang, and H. S. Zong, *Chinese Physics C* **43**, 063101 (2019), arXiv:1903.11243 [hep-ph].
- [60] C. D. Roberts and A. G. Williams, *Prog. Part. Nucl. Phys.* **33**, 477 (1994), arXiv:hep-ph/9403224.
- [61] C. D. Roberts and S. M. Schmidt, *Prog. Part. Nucl. Phys.* **45**, S1 (2000), arXiv:nucl-th/0005064.
- [62] P. Maris and C. D. Roberts, *Int. J. Mod. Phys. E* **12**, 297 (2003), arXiv:nucl-th/0301049.
- [63] R. Alkofer, *Phys. Rept.* **353**, 281 (2001), arXiv:hep-ph/0007355.
- [64] A. Bashir, L. Chang, I. C. Cloët, B. El-Bennich, Y. X. Liu, C. D. Roberts, and P. C. Tandy, *Commun. Theor. Phys.* **58**, 79 (2012), arXiv:1201.3366.
- [65] I. C. Cloet and C. D. Roberts, *Prog. Part. Nucl. Phys.* **77**, 1 (2014), arXiv:1310.2651 [nucl-th].
- [66] L. Chang, Y. X. Liu, and C. D. Roberts, *Phys. Rev. Lett.* **106**, 072001 (2011), arXiv:1009.3458.
- [67] S. X. Qin, L. Chang, Y. X. Liu, C. D. Roberts, and S. M. Schmidt, *Phys. Lett. B* **722**, 384 (2013), arXiv:1302.3276 [nucl-th].
- [68] S. X. Qin, L. Chang, Y. X. Liu, C. D. Roberts, and D. J. Wilson, *Phys. Rev. C* **84**, 042202 (2011), arXiv:1108.0603.
- [69] S. X. Qin, L. Chang, Y. X. Liu, and C. D. Roberts, *Phys. Rev. D* **84**, 014017 (2011), arXiv:1010.4231.
- [70] C. S. Fischer, *Phys. Rev. Lett.* **103**, 052003 (2009), arXiv:0904.2700.
- [71] C. S. Fischer and J. A. Mueller, *Phys. Rev. D* **80**, 074029 (2009), arXiv:0908.0007 [hep-ph].
- [72] E. Gutierrez, A. Ahmad, A. Ayala, A. Bashir, and A. Raya, *J. Phys. G* **41**, 075002 (2014), arXiv:1304.8065 [hep-ph].
- [73] B. Wang, Z. F. Cui, W. M. Sun, and H. S. Zong, *Few Body Syst.* **55**, 47 (2014), arXiv:1404.3073 [hep-ph].

- [74] K. L. Wang, Y. X. Liu, L. Chang, C. D. Roberts, and S. M. Schmidt, *Phys. Rev. D* **87**, 074038 (2013), [arXiv:1301.6762 \[nucl-th\]](#).
- [75] F. Gao and Y. X. Liu, *Phys. Rev. D* **94**, 076009 (2016).
- [76] N. Haque, M. G. Mustafa, and M. Strickland, *Phys. Rev. D* **87**, 105007 (2013).
- [77] R. Contant and M. Q. Huber, *Phys. Rev. D* **96**, 074002 (2017).
- [78] J. Madsen, *Phys. Rev. Lett.* **85**, 4687 (2000), [arXiv:hep-ph/0008217](#).
- [79] G. Lugones and A. G. Grunfeld, *Phys. Rev. C* **103**, 035813 (2021), [arXiv:2010.06098](#).
- [80] F. Gao and J. M. Pawłowski, *Phys. Rev. D* **102**, 034027 (2020).
- [81] W. J. Fu, J. M. Pawłowski, and F. Rennecke, *Phys. Rev. D* **101**, 054032 (2020).
- [82] M. S. Abdallah *et al.* (STAR), (2021), [arXiv:2105.14698](#).
- [83] A. Pandav (STAR), *Nuclear Physics A* **1005**, 121936 (2021).
- [84] T. Nonaka (STAR), *Nuclear Physics A* **1005**, 121882 (2021).
- [85] A. Bazavov *et al.* (HotQCD Collaboration), *Phys. Rev. D* **101**, 074502 (2020).
- [86] W. J. Fu, X. Luo, J. M. Pawłowski, F. Rennecke, R. Wen, and S. Yin, (2021), [arXiv:2101.06035 \[hep-ph\]](#).